# Morphometric analysis of Martian valley network basins using a circularity function

Wei Luo

Department of Geography, Northern Illinois University, DeKalb, Illinois, USA

Alan D. Howard

Department of Environmental Sciences, University of Virginia, Charlottesville, Virginia, USA

[1]  This paper employs a circularity function to quantify the internal morphology of Martian watershed basins in Margaritifer Sinus region and to infer the primary erosional processes that led to their current geomorphologic characteristics and possible climatic conditions under which these processes operated. The circularity function describes the elongation of a watershed basin at different elevations. We have used the circularity functions of terrestrial basins that were interpreted as having been modified by (1) erosion related to primarily groundwater sapping and (2) erosion related to primarily rainfall and surface run-off, as well as the circularity functions of cratering basins on the Moon, in order to formulate discriminant functions that are able to separate the three types of landforms. The spatial pattern of the classification of Martian basins based on discriminant functions shows that basins that look morphologically similar to terrestrial fluvial basins are mostly clustered near the mainstream at low elevation, while those that look morphologically similar to terrestrial basins interpreted as groundwater sapping origin are located near the tributaries and at higher elevation. There are more of the latter than the former. This spatial distribution is inconsistent with a continuous Earth-like warm and wet climate for early Mars. Instead, it is more aligned with an overall early dry climate punctuated with episodic wet periods. Alternatively, the concentrated erosion in the mainstream could also be caused by a change of water source from rainfall to snowfall or erosion cut through a duricrust layer.

**Citation:**  Luo, W., and A. D. Howard (2005), Morphometric analysis of Martian valley network basins using a circularity function, *J. Geophys. Res.*, *110*, E12S13, doi:10.1029/2005JE002506.

## 1.  Introduction

[2]  The origin of the valley networks has been debated since their discovery because whether they were formed predominantly by groundwater sapping or surface fluvial runoff has very important climatic, geologic and exobiologic implications [e.g., *Sharp and Malin*, 1975; *Pieri*, 1976, 1980; *Carr and Clow*, 1981; *Carr*, 1999; *Baker*, 1982, 1990; *Higgins*, 1982; *Mars Channel Working Group*, 1983; *Laity and Malin*, 1985; *Gulick and Baker*, 1989; *Haberle*, 1998; *Malin and Carr*, 1999; *Grant*, 2000; *Malin and Edgett*, 2000; *Goldspiel and Squyres*, 2000; *Williams and Phillips*, 2001; *Cabrol and Grin*, 2001; *Gulick*, 2001; *Craddock and Howard*, 2002; *Carr and Head*, 2003; *Hynek and Phillips*, 2003; *Craddock et al.*, 2003; *Stepinski and Collier*, 2004; *Howard et al.*, 2005]. Groundwater sapping can be loosely defined as erosion by groundwater that emerges as seeps and springs. This process often generates landforms that are characteristically different from fluvial landforms formed by erosion from surface rainfall-runoff [e.g., *Laity and Malin*, 1985]. These characteristics include U-shaped cross-sections, amphitheater termination, and low drainage density. Such features have been observed in valley networks on Mars. The instability of liquid water under current cold and dry Martian climatic conditions and the fact that most valley networks cut into the ancient cratered southern highland have led many researchers to believe that valley networks were formed primarily or exclusively by groundwater sapping. Hydrothermal circulation is often invoked to explain the groundwater recharge and the implication is that climate has always been cold and dry [*Pieri*, 1976, 1980; *Carr and Clow*, 1981; *Baker and Partridge*, 1986; *Brakenridge*, 1990; *Baker et al.*, 1992; *Goldspiel et al.*, 1993; *Carr and Chuang*, 1997].

[3]  However, the groundwater sapping landforms on Earth often occur in areas with permeable sandstone overlying friable aquicludes and surface runoff is necessary to remove the debris generated by groundwater sapping for sapping to continue [e.g., *Dunne*, 1990; *Craddock and Howard*, 2002]. The debate has recently shifted from favoring a groundwater sapping origin to realizing more

and more the importance of fluvial surface runoff and by inference at least some precipitation on early Mars, implying a warm and wet climate [e.g., *Craddock and Howard*, 2002; *Hynek and Phillips*, 2003; *Kerr*, 2003; *Harrison and Grimm*, 2005; *Irwin et al.*, 2005]. Nevertheless the paleoclimatic conditions during early Mars remain a key unresolved issue in the geologic history of the planet.

[4] Two main hypotheses exist: (1) it was warm and wet during the Noachian when precipitation and runoff and thus fluvial activities were widespread and gradually changed to present cold and dry conditions as the atmosphere lost most of its $CO_2$ [e.g., *Fanale*, 1976; *Pollack*, 1979; *Pollack et al.*, 1987; *Fanale et al.*, 1992]; (2) alternatively, warm and wet periods may have been infrequent and short-lived events superimposed on a generally cold and dry early climate. These intensive episodic rainfall events could be caused by large impacts in the 100 km+ diameter range that may have melted or evaporated subsurface ice and injected water into the atmosphere [*Carr*, 1989; *Segura et al.*, 2002; *Grant and Schultz*, 1990; *Colaprete et al.*, 2004]; or they could be correlated with brief optimal periods associated with the pronounced quasi-cyclic climatic variation of Mars [*Laskar et al.*, 2004]. The first hypothesis is the simplest but has the problems of not being able to reconcile with the reduced luminosity of the young Sun [*Kasting*, 1991], the lack of detectable carbonate deposits from remote sensing, and unweathered minerals identified from Mars Global Surveyor (MGS) and Mars Odyssey [*Hamilton and Christensen*, 2005; *Hoefen et al.*, 2003]. The second hypothesis can address these problems but has its own problem regarding the relative timing of impact events and erosion events typically associated with Martian climate change [*Jakosky and Mellon*, 2004]. The purpose of this paper is to evaluate these two alternative climatic change scenarios and other associated geologic conditions under which the valley networks were formed from the perspective of quantitative morphometric analysis at watershed basin scale.

## 2. Previous Morphometric Analysis at Watershed Basin Scale

[5] Most previous morphometric analyses were based on arbitrary areas or individual channel segments [e.g., *Carr and Chuang*, 1997; *Williams and Phillips*, 2001; *Hynek and Phillips*, 2003]. Using watershed basin as a basic unit in morphometric analysis is the most logical choice because all hydrologic and geomorphic processes occur within the watershed [*Singh*, 1992, p. 47]. Another advantage is that the overall basin-scale features could have survived the postformational degradation by cratering, eolian, and mass-wasting processes, whereas the details of individual valley and channel morphology may likely be obscured by these processes. Thus the morphometric characteristics at the watershed basin scale may contain important information regarding its formation and development. In addition, obtaining quantitative morphometric parameters at watershed basin scale for Mars will allow more direct and meaningful comparison with terrestrial landform and better inferences of the processes.

[6] Using statistical attributes of basin hypsometric curves [*Harlin*, 1978; *Luo*, 1998] and discriminant analysis technique, *Luo* [2000, 2002] was able to identify Martian

basins in Margaritifer Sinus region that look morphologically similar to terrestrial basins attributed to groundwater sapping and those that look morphologically similar to highly dissected terrestrial fluvial basins [*Luo*, 2002]. The result showed that both sapping-like and fluvial-like signatures were present in the Martian landform and there were more sapping-like basins than fluvial-like basins, consistent with a precipitation recharged groundwater sapping origin [*Baker and Partridge*, 1986; *Grant*, 2000; *Williams and Phillips*, 2001]. However, the spatial patterns of the classification were spatially disjointed and mixed, which prevented definitive process interpretations. This may be partially attributed to low resolution of the data used (1.86 km/pixel), not considering the effect of impact cratering [*Fortezzo and Grant*, 2004], and the basin boundaries that were extracted based on an arbitrary contributing area threshold of 5000 pixels. We have subsequently addressed all these issues later but discovered that hypsometric analysis cannot separate the sapping and cratering landforms very well. *Stepinski and Coradetti* [2004] developed a circularity function that is somewhat similar to a hypsometric curve but appears to be more diagnostic of the internal erosional processes of a basin. Using a Self Organization Map (SOM) technique to classify the basins based on the circularity function, they discovered that the Martian basins are quite different from the terrestrial basins except a few formed in hyperarid climate conditions [*Stepinski and Coradetti*, 2004], implying that the Martian basins were formed under a very arid environment.

## 3. Methods and Data Sources

[7] Given the success of circularity function in differentiating erosional processes of watershed basins, we adopted the circularity function as a means to quantify the morphometric shape of the basins. However, we chose a different classification approach, the (supervised) discriminant analysis approach, to classify the basins. The greatest advantage of this approach is that it can produce posteriori probability map which can serve as a measure of the relative importance of fluvial, sapping and cratering processes in generating the shape of the basin.

### 3.1. Circularity Function

[8] Whereas the hypsometric curve describes the relative area of a basin at different elevations, the circularity function of a basin measures the changes of the basin's elongation with elevation. The circularity function is defined in Figure 1, using a method similar to how a hypsometric curve is constructed. A horizontal plane at elevation $h$ cuts through the basin dividing the basin into two parts: one above plane and one below it. The circularity function at relative height $z = h/H$ ($0 \leq z \leq 1$, $H$ is the total relief of the basin) is based on area $a(z)$ and perimeter $p(z)$ of the part of the basin below the horizontal plane (the area shaded with hatch pattern):

$$C(z) = 4\pi a(z)/(p(z))^2 \qquad (1)$$

This is essentially the ratio of the area of the shaded area to the area of a circle whose circumference is equal to the perimeter of the shaded area. So for a perfect circle, $C = 1$;
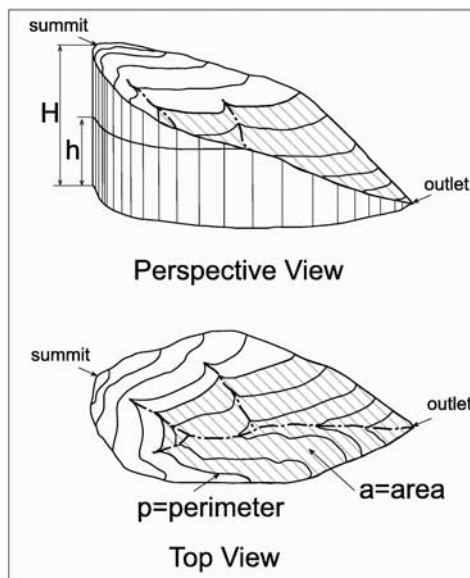
**Figure 1.** Schematic diagram showing the construction of circularity function. $C(z) = 4\pi a(z)/(p(z))^2$, $z = h/H$, where $z$ is the relative height, $H$ is the total relief, $a$ is the area of the shaded area, and $p$ is perimeter of the shaded area.

for an elongated shape, $C < 1$. The more elongated the shape is, the less the $C$ value. As $z$ changes from 0 to 1, a series of $C$ values form the circularity function or a circularity curve of the basin [*Stepinski and Coradetti*, 2004].

### 3.2. Data Source, Watershed Boundary Delineation, and Training Samples

[9] The digital elevation model (DEM) data used in this study and their source are summarized in Table 1. The terrestrial data were degraded to match the resolution of the Martian data. The lunar data for the heavily cratered highlands in the polar regions (>~65° latitudes) were derived from photogrammetric data and Clementine laser altimeter data [*Rosiek et al.*, 1999] and has a resolution of 1000 m, which is the best resolution currently available. (We have conducted test of degrading all terrestrial data to 1000 m resolution and the classification result are similar to those presented in the Results section in terms of the spatial patterns of the classification and probability map. Thus this resolution does not affect the result. In fact, using 30 m resolution terrestrial training samples also generated similar spatial pattern.)

[10] The watershed boundaries were delineated from these DEMs using the RiverTools software with the stan-

dard D8 algorithm [*O'Callaghan and Mark*, 1984; *Mark*, 1988; *Jenson and Domingue*, 1988]. We used the Strahler stream order rather than the contributing area as used by *Stepinski and Collier* [2004] as the control variable because this approach works better in areas where relief changes rapidly (personal communication with S. Peckham, 2005). The constant drop law, i.e., the average elevation drop of streams at different order is approximately constant [*Broscoe*, 1959], was used as an objective criterion to determine where the channels are [*Tarbonton et al.*, 1991] and all the pixels draining into the same channel segment is grouped as a subwatershed (we will refer to subwatershed as watershed or basin in this paper). We first assumed every cell was part of a channel and then computed the mean and standard deviation of the elevation drop of each order stream and the $t$ statistics. If the elevation drop of the 1st order stream was statistically different from the higher order streams, we removed (pruned) the 1st order stream and the original 2nd order stream now becomes the new 1st order stream and so on. We successively pruned the lower order streams [*Peckham*, 1995] until the elevation drop of the new 1st order stream was not statistically different from the higher order streams, i.e., the $t$ statistic was less than 2 [*Tarbonton et al.*, 1991]. Even though we know there is no water erosion on the Moon, we can still apply the same algorithm to delineate "watersheds" on the lunar landform [*Stepinski and Collier*, 2004; *Fortezzo and Grant*, 2004]. This allows us to extract the morphologic signature of landforms created by pure impact cratering.

[11] Figure 2 shows the locations of the training basins. The top panel shows terrestrial basins that have been interpreted to be formed primarily by groundwater sapping (filled black areas in Figure 2) and fluvial surface runoff (open areas). The bottom panel shows basins delineated at the polar regions of the Moon. The statistics of areas of the sample basins are shown in Table 2.

[12] The training basins that have been interpreted to be formed primarily by groundwater sapping are located in Colorado Plateau [*Laity and Malin*, 1985], in Florida panhandle [*Schumm et al.*, 1995] and in northern Chile [*Hoke et al.*, 2004]. These basins have characteristic morphologies such as amphitheater channel head, low drainage density, high and steep valley sidewalls. There is clear evidence that groundwater sapping played an important role in forming such characteristic morphology. However, several authors have also realized that such morphology, particularly the box canyons in Navajo Sandstone in Colorado Plateau, requires a specific stratigraphic setting, i.e., a massively bedded, moderately cemented, poorly jointed, permeable flat-lying sandstone over an easily eroded aquiclude [e.g., *Dunne*, 1990; Lamb et al., manuscript in preparation, 2005]. In addition, the surface runoff is needed

**Table 1.** Topographic Data Source, Resolution, and Focused Areas

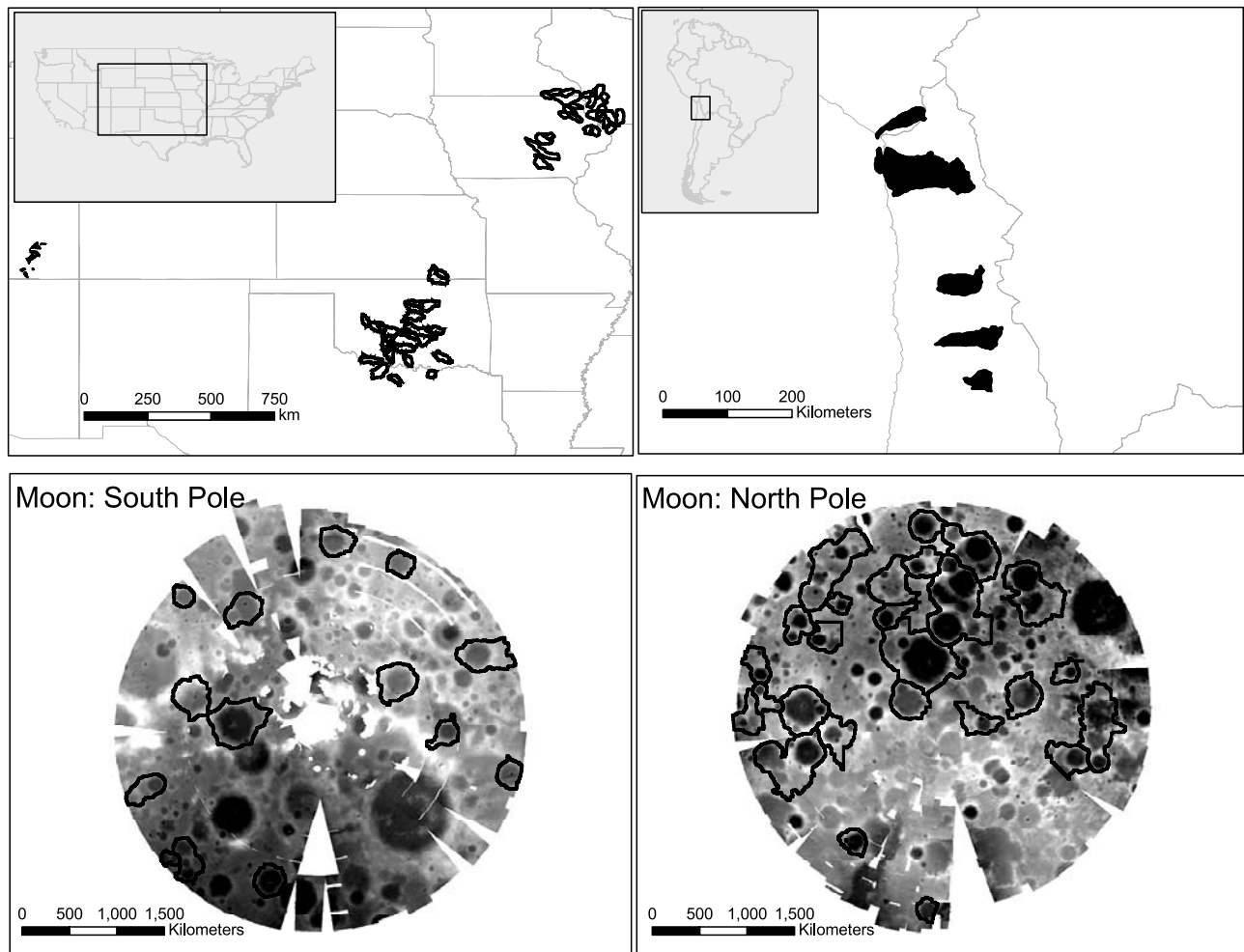| Planet | Data Set, Source | Resolution, m | Focused Study Areas |
|---|---|---|---|
| Earth | SRTM, USGS | ~90 m/pixel original resampled to ~450 m/pixel | Colorado Plateau, UT, Chile WI, IL, OK, AL |
| Moon | Clementine, USGS | ~1000 m/pixel | South and North poles |
| Mars | MOLA 1/128 degree DEM | ~463 m/pixel at equator | Margaritifer Sinus |

**Figure 2.** Locations of the training basins. Top panels: terrestrial basins that were interpreted as primarily formed by groundwater sapping processes (shown as black filled areas) and those that were interpreted as primarily formed by surface fluvial erosion (shown as open areas). Bottom panels: basins delineated from lunar topographic data at south and north poles.

to remove debris created by groundwater sapping at the base of the slope for groundwater sapping process to continue to operate [*Howard and Kochel*, 1988; *Craddock and Howard*, 2002]. Therefore, for the rest of paper, we will refer to this type of basin as "canyon-like" basins, a process neutral term. The training basins that have been interpreted as primarily formed by surface fluvial runoff (mostly located in Okalahoma [*Harlin*, 1982] and Iowa [*Bridges*, 1990]) have high drainage density and are more uniformly dissected throughout the basin. We will refer to this training class as "well-dissected" basins. We will discuss the process and climate implication in the Interpretation and

Discussion section. For the basins delineated from the Moon, we simply call them cratering basins.

[13] Figure 3 shows the average, maximum, minimum and standard deviation of the circularity curve of the three classes of training sample. There is a characteristic shape for well-dissected basins, which look like a flattened letter "J", with generally low $C$ values in the lower part of the basin and high $C$ values in the higher part of the basin. The lowest $C$ is at around relative elevation 0.3. The standard deviation is also generally low (less than 0.1). This is resulted from elongation of the lower parts of the basin along the major streams by concentrated fluvial erosion there. The canyon-

**Table 2.** Statistics of the Basin Area of the Training Samples and Martian Study Area[a]

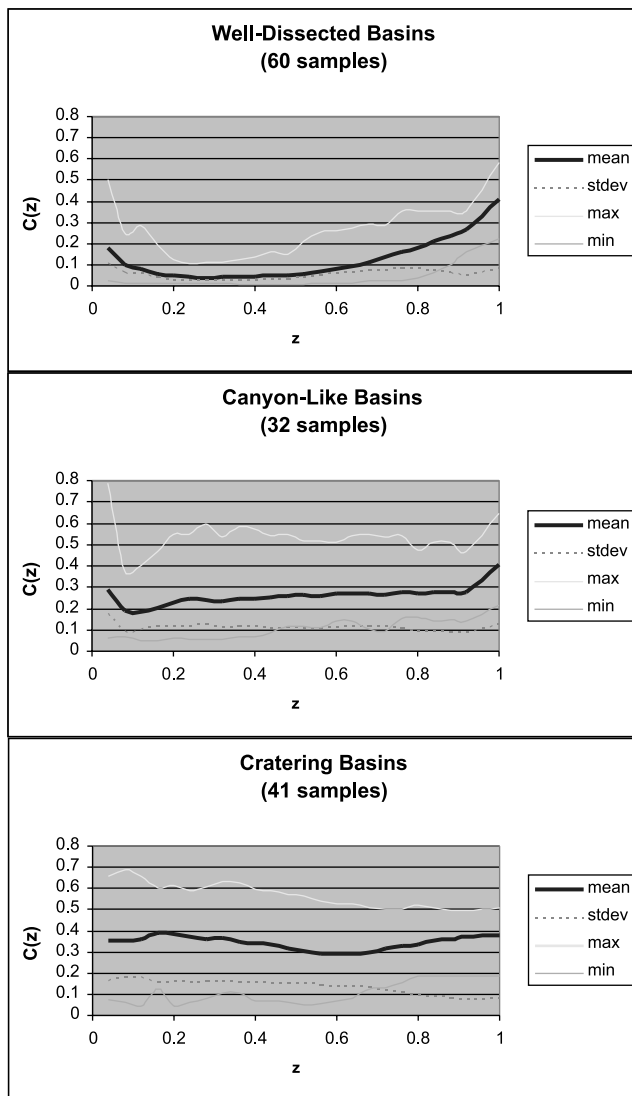| Group or Area | Mean | Standard Deviation | Minimum | Maximum | Number of Samples |
|---|---|---|---|---|---|
| Well-dissected | 1.0E+03 | 6.0E+02 | 2.6E+02 | 2.9E+03 | 60 |
| Canyon-like | 7.3E+02 | 7.9E+02 | 4.6E+01 | 2.7E+03 | 32 |
| Cratering | 1.4E+04 | 9.7E+03 | 2.7E+03 | 4.3E+04 | 41 |
| Margaritifer Sinus | 1.7E+04 | 1.2E+04 | 4.3E+02 | 6.5E+04 | 106 |

[a]Units are km$^2$.

**Figure 3.** The mean, maximum, minimum, and standard deviation of the circularity function curve of the three classes of training basins.

like basins show fluctuation in $C$ values with a slight increasing trend with relative elevation. The lowest $C$ is around relative elevation 0.1. The stand deviation is around 0.1. Cratering basins show a high $C$ value throughout all elevation with no clear trend and lowest $C$ at around relative elevation 0.6. The stand deviation is also the highest of all, particularly in the lower elevations. This is expected because craters are of circular shape.

### 3.3. Discriminant Analysis

[14] Figure 4 shows the circularity function for the Martian basins in Margaritifer Sinus area, which were similarly delineated using RiverTools and their sizes are shown in Table 2. The purpose of the discriminant analysis is to classify these Martian basins into well-dissected, canyon-like, and cratering classes based on the characteristics of each training class shown in Figure 3. In order to do that, we first normalize the circularity function by the whole basin circularity, $C_n(z) = C(z)/C(1)$. This disengages the

internal basin morphology from the external basin shape [*Stepinski and Coradetti*, 2004] and thus removes the influence of external basin shape on the circularity function and allows for comparability between different basins to reveal its internal structure and, by inference, the erosional processes.

[15] Next, the normalized circularity functions were sampled at every 1/25 interval of relative height (0.04, 0.08, ... 1), forming 24 variables for each basin ($v_1$, $v_2$, ..., $v_{24}$) (see Figure 5). The last variable $v_{24}$ was excluded from analysis because it is always equal to 1 and thus does not offer any discriminant power. Statistical $t$-tests showed that the differences between the three training classes on all of the remaining 23 variables are statistically significant. Thus all of the 23 variables entered discriminant analysis. The resulting discriminant function was first applied back to the training samples themselves and misclassified samples were re-moved. This process was iterated until all the training samples were correctly classified. This initial iterative selection process ensures that the samples were truly end-members in the parameter space. Curves shown in Figure 3 and statistics shown in Table 2 were generated from the samples left after this initial iterative removing process. We will refer to this set of samples as the training sample hereafter. The discriminant analysis was completed in SAS software.

## 4. Results
### 4.1. Sensitivity Analysis and Accuracy Estimate Based on Training Data

[16] In order to estimate the accuracy of the classification, we randomly selected 25% of the training samples from each class as crossvalidate (holdout) samples (i.e., 15, 8, and 10 samples for well-dissected, canyon-like and crater-ing classes, respectively, cf. number of samples in Table 2) and used the remaining 75% of the samples as analysis samples to derive the discriminant functions [*Huberty*, 1994, p. 88]. The resulting discriminant functions were then applied to classify the holdout samples (which did not participate in deriving the functions). By comparing the classification result with their known classes (crossvalidate), the classification accuracy for each class is estimated as the ratio of the number of correctly classified samples in that class to the true number of samples in that class. To test the sensitivity of the discriminant analysis result on different training samples, we repeated the above process 5 times,
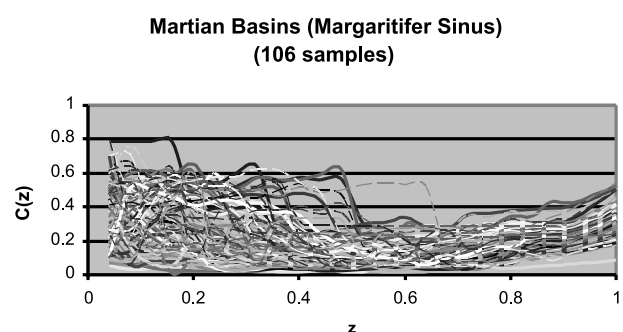
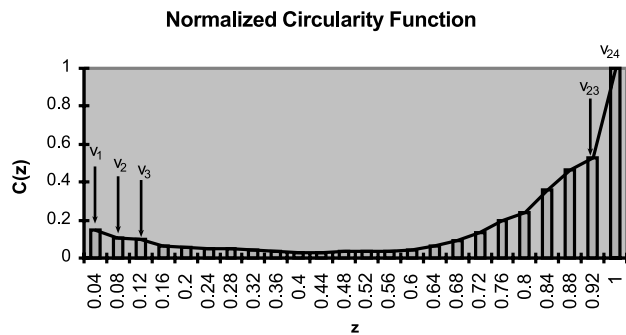**Figure 4.** The circularity function curve for the Martian basins.

**Normalized Circularity Function**



**Figure 5.** Diagram illustrating the variables used in discriminant analysis.

**Table 3.** Classification Accuracy Estimate[a]

| Class | Well-Dissected | Canyon-Like | Cratering |
|---|---|---|---|
| Mean | 97.3 | 95.0 | 90.0 |
| Std. Dev. | 3.7 | 6.8 | 10.0 |
| Maximum | 100.0 | 100.0 | 100.0 |
| Minimum | 93.3 | 87.5 | 80.0 |

[a]Units are percent.

i.e., 5 different subsets of randomly selected holdout and analysis samples (from the training samples) were used. Table 3 summarizes the statistics of the accuracy estimate based on the 5 sensitivity tests. On average, over 90% of the basins were correctly classified, with a minimum accuracy of 80%. For each basin, three posteriori probabilities were generated from each discriminant analysis and the basin is classified into a class that has the largest probability. The means of posteriori probability of each class in each of the 5 random tests were all above 0.8. The leave-one-out method, which involves iteratively removing 1 sample from the analysis and applying the discriminant functions determined from the remaining (n-1) samples back to classify that removed sample [*Huberty*, 1994, p. 88], resulted in even higher accuracy (>95%). So random sensitivity tests show that the results are very similar against different training data and a conservative accuracy estimate is 80%.

[17] We have also conducted an unsupervised classification of the training samples using the Self Organization Map (SOM) and Ward Clustering method [*Stepinski and Coradetti*, 2004, and references therein]. Over 80% of samples in each class are correctly classified, consistent with estimate based on sensitivity tests, and those misclassified samples were mostly located close to the border between classes in the SOM.

## 4.2. Results of Application to Mars Data

[18] The discriminant functions derived from the above 5 sensitivity tests were applied to the Martian basins data (as shown in Figure 4) to classify them into the 3 classes, which generated 5 sets of results. Mapping the spatial distribution of classifications showed that the 5 sets of results had very similar spatial pattern, even though there were slight differences in the posteriori probability of each basin and the membership of a few basins. For each set of result, each basin had a posteriori probability of belonging to each of the 3 classes. For each basin, we took the average posteriori probability of the 5 results as the probability of a basin belonging to a class and classify the basin to a class that has the maximum average posteriori probability. The statistics of total area and average probability of the classification result are summarized in Table 4. There are more basins classified as canyon-like than those classified as well-dissected (both in terms of number and area of basins), similar to the findings of *Luo* [2002]. The average proba-

bility is also about 0.8, consistent to the accuracy estimate based the 5 random crossvalidate tests.

[19] The spatial distribution is shown in Figure 6a with a Viking image mosaic in the background and the Strahler stream order in the foreground. Unlike the result of *Luo* [2002], with a few exceptions, basins of the same class are generally spatially adjacent to each other (Figure 6a). This may be due to the facts that we are using higher resolution DEM and that watershed boundaries were more objectively extracted. It is very striking to notice that the well-dissected basins (blue) mostly coincide with high order streams, whereas the canyon-like basins (green) mostly coincide with low order streams. On average, canyon-like basins are higher in elevation than well-dissected basins ($-330$ m versus $-1200$ m) and the difference is statistically significant. Since the classification is only based on the maximum probability, to show more subtle variation of the degree of resemblance of each basin to the well-dissected and the canyon-like training classes, we map the posteriori probability in Figure 6b. It is clear in the probability map that basins that look more morphologically similar to the well-dissected basins cluster around main (high order) stream and the basins that look more morphologically like canyon-like basins are more "pervasive" throughout the area. To illustrate this feature more quantitatively, we calculated the shortest distance of each basin's centroid to the mainstream (4th order stream in this case). Figure 7 shows a plot of the probability of each basin belonging to the well-dissected versus its centroid's nearest distance to the mainstream, along with a 5-point moving average and linear fit lines. Although the scatter in the linear fit is great ($R^2 = 0.16$), the regression relationship is statistically significant (F = 20.9, p = 1.3e − 5). The general trend is clear: the farther way a basin is from the mainstream, the lower its probability of belonging to the well-dissected class.

## 4.3. Assessment of Postformational Modification on Circularity Function

[20] The topography we observe today resulted from a combination of the erosional processes that formed the valley networks and the modifications from burial and infill from masswasting and eolian processes after the major erosion stopped. If such postformational modification is severe, it could prevent us from interpreting valley forming

**Table 4.** Statistics of Classification Result of Martian Basins

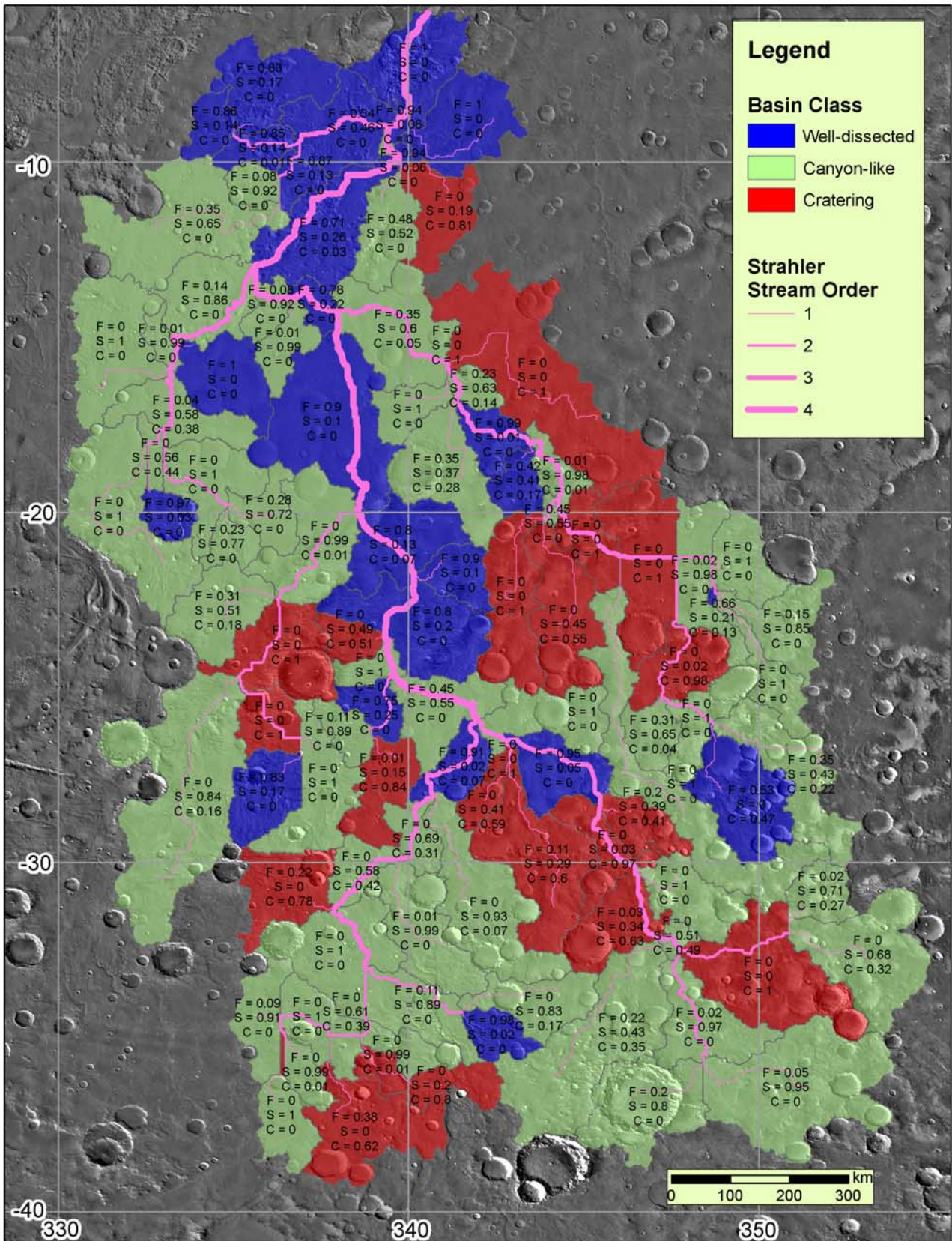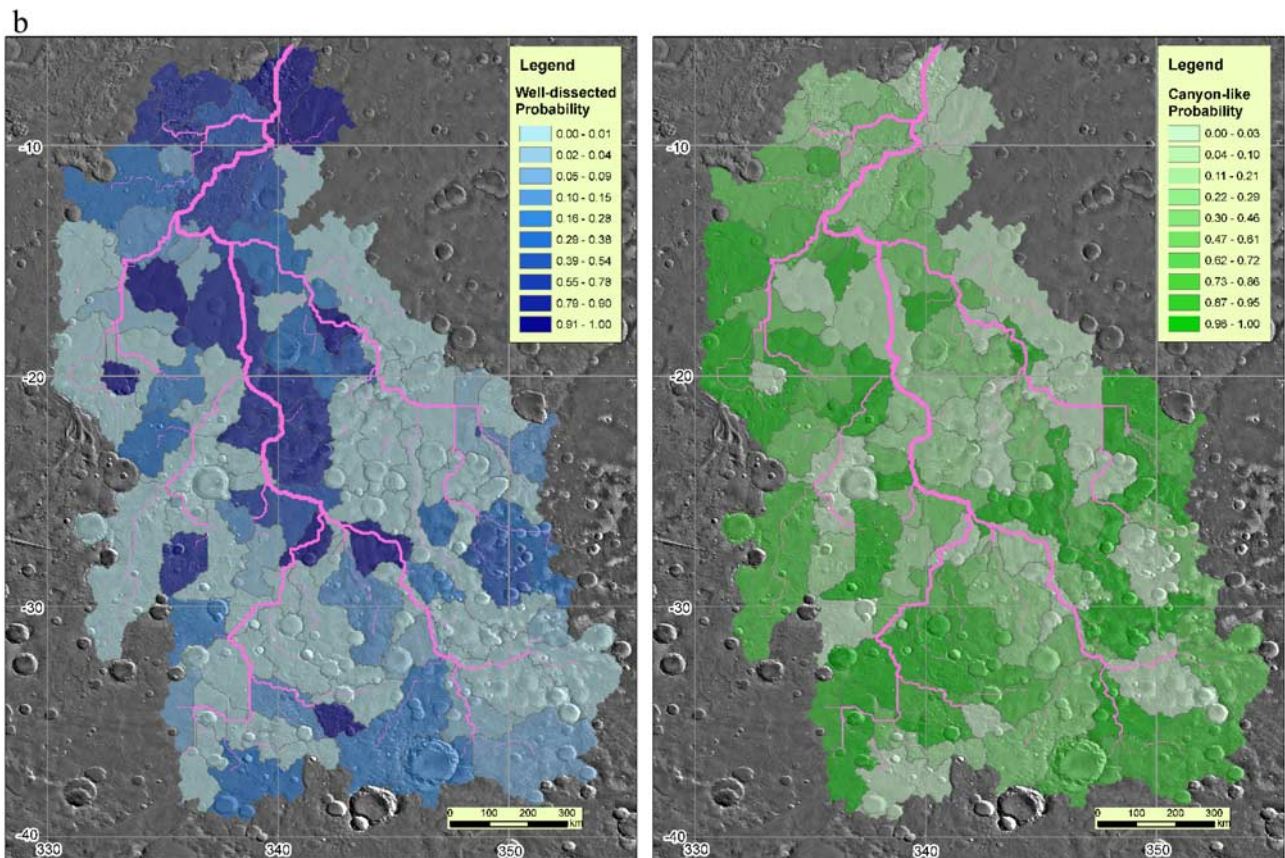| Class | Total Area in Class, km$^2$ | Number of Basins in Class | Average Prob. in Class | Std. Dev. | Min. | Max. |
|---|---|---|---|---|---|---|
| Well-dissected | 3.6E+05 | 26 | 0.834 | 0.156 | 0.419 | 0.999 |
| Canyon-like | 9.9E+05 | 58 | 0.816 | 0.198 | 0.365 | 1.000 |
| Cratering | 4.1E+05 | 22 | 0.821 | 0.203 | 0.407 | 1.000 |

a



**Figure 6**

**Figure 6.** (continued)

processes. To evaluate this concern, we applied the discriminant function to the filled DEM created in the process of delineating watershed, which has a mean fill of about 100 m, with a standard deviation of 300 m and maximum of up to 3 km. The result from the filled DEM shows that although the class membership of some individual basins do change, the spatial distribution pattern of the probability map is generally very similar to that generated from the original unfilled DEM, especially the correlation of well-dissected basins with mainstream at the lower elevation. Detailed valley morphology analysis based on width to depth ratio of *Williams and Phillips* [2001] suggests that such modification is minimal. *Goldspiel et al.* [1993] estimated less than 20 m of eolian infill based on small crater rim heights preserved on valley network floors. As argued in section 2, the morphometric signature from valley forming process contained in the circularity function at *basin scale* would have been minimally affected by such small postformational modification. Based on this assessment and the sensitivity analysis and accuracy estimate presented earlier, we are reasonably confident about the general spatial pattern of the morphometric characteristics presented in section 4.2.

## 5. Interpretation and Discussion

[21] Subsurface groundwater sapping, the process responsible for some canyon-like morphology on Earth, is a less effective erosional process than surface runoff erosion generated from atmospheric precipitation, as the former process can only operate at limited sites with large enough groundwater discharge rate [e.g., *Howard*, 1988]. The fact that this analysis show more canyon-like basins (see Table 4) suggests that groundwater sapping processes must have operated longer than the fluvial processes [*Luo*, 2002].

[22] If the climate of Mars were warm and wet with Earth-like widespread precipitation and surface runoff and fluvial erosion during the Noachian and gradually changed to present cold and dry conditions, we would expect to see a spatial pattern of more well-dissected basins everywhere (especially at high elevations due to orographic effect) and canyon-like basins only at the lower elevations as the

---

**Figure 6.** (a) Classification of basins in Margaritifer Sinus region. Background is the Viking image mosaic. Red, green, and blue colors show cratering, canyon-like, and well-dissected basin classes. Different thickness of pink lines indicates different Strahler stream orders. Numbers indicate the posteriori probability. (b) The posteriori probability of discriminant analysis for each basin shown as graduated color. Left is the probability of each basin belonging to well-dissected basin class, and right is the probability of each basin belonging to canyon-like basin class.
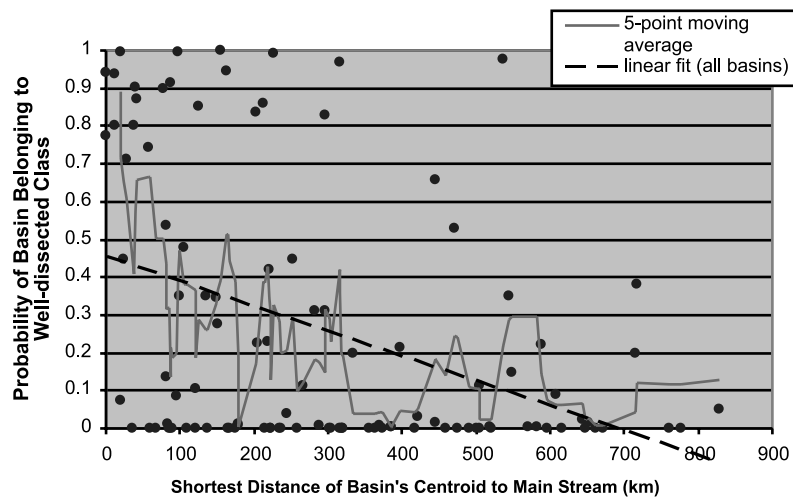
**Figure 7.** Scatterplot of a basin's probability belonging to well-dissected class versus the shortest distance of its centroid to the mainstream. Also shown are the 5-point moving average and the linear fit.

climate got drier and water table dropped. The result of this analysis is just the opposite: we see basins with high well-dissected probability clustered around mainstream at lower elevations and basins with high canyon-like probability spatially widespread and around low order stream at higher elevations (Figure 6).

[23] We suggest three process and environmental scenarios that appear to be consistent with the observed basin morphology. This morphologic pattern may be consistent with a dry climate throughout most of the Martian history but punctuated with periods of intermittent wet spells. During wetter periods, precipitation would infiltrate the highly permeable material, leaving less fluvial signature at higher elevations and tributary areas. The infiltrated precipitation water would seep out to the surface at a few intermediate order streams with large enough discharge forming canyon-like basins. Further downstream, the water flowing down from seepage sites at higher elevation and surface water routed from upstream would accumulate to large quantity, causing concentrated erosion in the lower reaches of the drainage, particularly the mainstream, resulting in the elongated circularity function there. Groundwater sapping erosion might have continued during relatively dry periods in larger valleys helping to form canyon-like basins. The episodic rainfall events could recharge the groundwater table to keep it close to the surface and remove the debris formed by groundwater sapping process. We note, however, that crater rims and other high-relief divides were also modified by erosion during the Noachian. Denudation of crater rims resulted in significant infilling of crater floors and inter-crater basins [*Craddock and Howard*, 2002; *Forsberg-Taylor et al.*, 2004]. But this modification appears to have involved short-distance transport and was insufficient to create well-defined integrated valleys in headwaters or to mask the overall cratering topographic signature of portions of the drainage basins (Figure 6a).

[24] This interpretation is corroborated by several other studies, e.g., *Stepinski and Coradetti* [2004], *Stepinski and Stepinski* [2005], *Irwin et al.* [2005], and *Howard et al.*

[2005]. In particular, *Howard et al.* [2005] reported a late stage fluvial incision occurred primarily in the downstream portions of drainage networks and only affected higher-order streams. Besides the temporal episodic warm and wet conditions possibly triggered by orbital change, large impacts, intense volcanism, or outflow floods spreading water across the northern lowlands, *Howard et al.* [2005] also pointed out two other alternative environmental scenarios that might explain this concentrated erosion in mainstreams: (1) a change from rainfall to snowmelt runoff, and (2) formation and subsequent erosion of regional duricrust. Both scenarios would cause a reduction of size or quantity of supplied sediment or increased magnitude of fluvial discharge, leading to concentrated incision in the mainstreams [*Howard et al.*, 2005], consistent with the spatial pattern revealed by this study. The snowmelt runoff scenario would mean a cold and wet climate but would still require some warm episodes to make the snowmelt, which is very similar to our favored scenario of episodic warm and wet periods punctuating a generally dry climate. The climatic implication of the duricrust scenario is less clear. In any case, all three scenarios can possibly generate the spatial pattern of basin scale morphometric characteristics revealed in this study. We need additional information to distinguish between these scenarios or combination of scenarios and to constrain the timing and the magnitude of the episodic wet periods.

## 6. Conclusion

[25] We used the circularity functions of terrestrial canyon-like basins that have been interpreted to be formed primarily by groundwater sapping, basins formed by surface fluvial erosion, as well as cratering basins on the Moon to derive discriminant functions that are able to separate the three types of landforms. We then applied discriminant functions to Martian data to classify the Martian basins into these 3 classes. The posteriori probability from discriminant analysis can be used to interpret the relative importance of distributed surface fluvial erosion versus concentrated can-

yon-like incision (possibly due to groundwater sapping) in forming the valley network basins. The spatial pattern of the classification probability map shows that basins that look morphologically similar to terrestrial fluvial basins are mostly clustered near the mainstream at low elevations while those that look morphologically similar to terrestrial canyon-like basins interpreted as groundwater sapping origin are located near the tributaries and at higher elevation. This is contrary to what one would expect if the climate on Mars was warm and wet and supported Earth-like precipitation and fluvial activities during the Noachian. We suggest three process and environmental scenarios that appear to be consistent with the observed spatial pattern of basin morphology: (1) a generally dry and cold climate punctuated with discrete episodes or isolated events of warm and wet condition in its history, perhaps created by ancient large impacts or during those brief optimal periods associated with the pronounced quasi-cyclic climatic variation of Mars; (2) a change from rainfall to snowmelt runoff; and (3) formation and subsequent erosion of regional duricrust. However, more information is needed to constrain the timing and intensity of such wet events, and to distinguish between the three possible scenarios.

# References

Baker, V. R. (1982), *The Channels of Mars*, 198 pp., Univ. of Tex. Press, Austin.

Baker, V. R. (1990), Spring sapping and valley network development, in *Groundwater Geomorphology: The Role of Subsurface Water in Earth-Surface Processes and Landform*, edited by C. G. Higgins and D. R. Coates, *Spec. Pap. Geol. Soc. Am.*, 252, 235–265.

Baker, V. R., and J. B. Partridge (1986), Small Martian valleys: Pristine and degraded morphology, *J. Geophys. Res.*, 91(3), 3561–3572.

Baker, V. R., M. H. Carr, V. C. Gulick, C. R. Williams, and M. S. Marley (1992), Channels and valley network, in *Mars*, edited by H. H. Kieffer et al., pp. 493–522, Univ. of Ariz. Press, Tucson.

Brakenridge, G. R. (1990), The origin of fluvial valleys and early geologic history, aeolis quadrangle, Mars, *J. Geophys. Res.*, 95(B11), 17,289–17,308.

Bridges, E. M. (1990), *World Geomorphology*, pp. 84–87, Cambridge Univ. Press, New York.

Broscoe, A. J. (1959), Quantitative analysis of longitudinal stream profiles of small watersheds, *Off. Naval Res. Proj. NR 389-042, Tech. Rep. 18*, Dep. of Geol., Columbia Univ., New York.

Cabrol, N. A., and E. A. Grin (2001), Composition of the drainage network on early Mars, *Geomorphology*, 37(3), 269–289.

Carr, M. H. (1989), Recharge of the early atmosphere of Mars by impact-induced release of $CO_2$, *Icarus*, 79(2), 311–327.

Carr, M. H. (1999), Global history of water and climate, in *Fifth International Conference on Mars*, Lunar and Planet. Inst., Houston, Tex.

Carr, M. H., and F. C. Chuang (1997), Martian drainage densities, *J. Geophys. Res.*, 102, 9145–9152.

Carr, M. H., and G. D. Clow (1981), Martian channels and valleys: Their characteristics, distribution, and age, *Icarus*, 48(1), 91–117.

Carr, M. H., and J. W. Head III (2003), Basal melting of snow on early Mars: A possible origin of some valley networks, *Geophys. Res. Lett.*, 30(24), 2245, doi:10.1029/2003GL018575.

Colaprete, A., R. M. Haberle, T. L. Segura, O. B. Toon, and K. Zahnle (2004), The effect of impacts on the early Martian climate, in *Second Conference on Early Mars*, Abstract 8016, Lunar and Planet. Inst., Houston, Tex.

Craddock, R. A., and A. D. Howard (2002), The case for rainfall on a warm, wet early Mars, *J. Geophys. Res.*, 107(E11), 5111, doi:10.1029/2001JE001505.

Craddock, R. A., R. P. Irwin III, and A. D. Howard (2003), Characteristics of Martian valley networks and the implications for past climates, *Lunar Planet. Sci.*, XXXIV, Abstract 1888.

Dunne, T. (1990), Hydrology, mechanics, and geomorphic implications of erosion by subsurface flow, in *Groundwater Geomorphology: The Role of Subsurface Water in Earth-Surface Processes and Landform*, edited by C. G. Higgins and D. R. Coates, *Spec. Pap. Geol. Soc. Am.*, 252, 11–28.

Fanale, F. P. (1976), Martian volatiles: Their degassing history and geochemical fate, *Icarus*, 28(2), 179–202.

Fanale, F. P., S. E. Postawko, J. B. Pollack, M. H. Carr, and R. O. Pepin (1992), Mars: Epochal climate change and volatile history, in *Mars*, edited by H. H. Kieffer et al., pp. 1135–179, Univ. of Ariz. Press, Tucson.

Forsberg-Taylor, N. K., A. D. Howard, and R. A. Craddock (2004), Crater degradation in the Martian highlands: Morphometric analysis of the Sinus Sabaeus region and simulation modeling suggest fluvial processes, *J. Geophys. Res.*, 109, E05002, doi:10.1029/2004JE002242.

Fortezzo, C., and J. A. Grant (2004), Hypsometric analyses of Martian basins: A comparison to terrestrial, lunar and Venusian hypsometry, *Lunar Planet. Sci.* [CD-ROM], XXXV, Abstract 1647.

Goldspiel, J., and S. Squyres (2000), Groundwater sapping and valley formation on Mars, *Icarus*, 148(1), 176–192.

Goldspiel, J. M., S. W. Squyres, and D. G. Jankowski (1993), Topography of small Martian valleys, *Icarus*, 105, 479–500.

Grant, J. A. (2000), Valley formation in Margaritifer Sinus, Mars, by precipitation-recharged ground-water sapping, *Geology*, 28(3), 223–226.

Grant, J. A., and P. H. Schultz (1990), Gradational epochs on Mars: Evidence from west-northwest of Isidis Basin and Electris, *Icarus*, 84, 166–195.

Gulick, V. C. (2001), Origin of the valley networks on Mars: A hydrological perspective, *Geomorphology*, 37(3), 241–269.

Gulick, V., and V. R. Baker (1989), Fluvial valleys and Martian paleoclimates, *Nature*, 341(6242), 514–516.

Haberle, R. M. (1998), Early Mars climate models, *J. Geophys. Res.*, 103(E12), 28,467–28,480.

Hamilton, V. E., and P. R. Christensen (2005), Evidence for extensive, olivine-rich bedrock on Mars, *Geology*, 33(6), 433–436.

Harlin, J. M. (1978), Statistical moments of the hypsometric curve and its density function, *Math. Geol.*, 10(1), 59–72.

Harlin, J. M. (1982), Geology and geomorphology of the southern plains research watershed, *Okla. Geol. Notes*, 42, 168–178.

Harrison, K. P., and R. E. Grimm (2005), Groundwater-controlled valley networks and the decline of surface runoff on early Mars, *J. Geophys. Res.*, 110, E12S16, doi:10.1029/2005JE002455.

Higgins, C. G. (1982), Drainage systems developed by sapping on Earth and Mars, *Geology*, 10(3), 147–152.

Hoefen, T. M., R. N. Clark, J. L. Bandfield, M. D. Smith, J. C. Pearl, and P. R. Christensen (2003), Discovery of olivine in the Nili, Fossae region of Mars, *Science*, 302, 627–630.

Hoke, G. D., B. L. Isacks, T. E. Jordan, and J. S. Yu (2004), A groundwater sapping origin of the giant quebradas of northern Chile, *Geology*, 32(7), 605–608.

Howard, A. D. (1988), Groundwater sapping experiments and modeling, in *Sapping Features of the Colorado Plateau: A Comparative Planetary Geology Field Guide*, edited by A. D. Howard, R. C. Kochel, and H. R. Holt, *NASA Spec. Publ.*, NASA SP-491, 71–83.

Howard, A. D., and R. C. Kochel (1988), Introduction to cuesta landforms and sapping processes on the Colorado Plateau, in *Sapping Features of the Colorado Plateau: A Comparative Planetary Geology Field Guide*, edited by A. D. Howard, R. C. Kochel, and H. R. Holt, *NASA Spec. Publ.*, NASA SP-491, 6–56.

Howard, A. D., J. M. Moore, and R. P. Irwin III (2005), An intense terminal epoch of widespread fluvial activity on early Mars: 1. Valley network incision and associated deposits, *J. Geophys. Res.*, 110, E12S14, doi:10.1029/2005JE002459.

Huberty, C. J. (1994), *Applied Discriminant Analysis*, *Wiley Ser. Probab. Math. Stat.*, 466 pp., John Wiley, Hoboken, N. J.

Hynek, B. M., and R. J. Phillips (2003), New data reveal mature, integrated drainage systems on Mars indicative of past precipitation, *Geology*, 31(9), 757–760.

Irwin, R. P., III, R. A. Craddock, and A. D. Howard (2005), Interior channels in Martian valley networks: Discharge and runoff production, *Geology*, 33(6), 489–492, doi:10.1130/G21333.1.

Jakosky, B. M., and M. T. Mellon (2004), Water on Mars, *Phys. Today*, April.

Jenson, S. K., and J. O. Domingue (1988), Extracting topographic structure from digital elevation data for Geographic Information Analysis, *Photogramm. Eng. Remote Sens.*, 54(11), 1593–1600.

Kasting, J. F. (1991), $CO_2$ condensation and the climate of early Mars, *Icarus*, 94(1), 1–13.

Kerr, R. A. (2003), Running water eroded a frigid early Mars, *Science*, 300(6), 1496–1497.

Laity, J. E., and M. C. Malin (1985), Sapping processes and the development of theater-headed valley networks in the Colorado Plateau, *Geol. Soc. Am. Bull.*, *96*, 203–217.

Laskar, J., A. C. M. Correia, M. Gastineau, F. Joutel, B. Levrard, and P. Robutel (2004), Long term evolution and chaotic diffusion of the insolation quantities of Mars, *Icarus*, *170*, 343–364.

Luo, W. (1998), Hypsometric analysis with a Geographic Information System, *Comput. Geosci.*, *24*, 815–821.

Luo, W. (2000), Quantifying groundwater sapping processes with a hypsometric analysis technique, *J. Geophys. Res.*, *105*, 1685–1694.

Luo, W. (2002), Hypsometric analysis of Margaritifer Sinus and origin of valley networks, *J. Geophys. Res.*, *107*(E10), 5071, doi:10.1029/2001JE001500.

Malin, M. C., and M. H. Carr (1999), Groundwater formation of Martian valleys, *Nature*, *397*(6720), 589–591.

Malin, M. C., and K. S. Edgett (2000), Evidence for recent groundwater seepage and surface runoff on Mars, *Science*, *288*, 2330–2335.

Mark, D. M. (1988), Network models in Geomorphology, in *Modeling in Geomorphological Systems*, John Wiley, Hoboken, N. J.

Mars Channel Working Group (1983), Channels and valleys on Mars, *Geol. Soc. Am. Bull.*, *94*, 1035–1054.

O'Callaghan, J. F., and D. M. Mark (1984), The extraction of drainage networks from digital elevation data, *Comput. Vision Graphics Image Process.*, *28*, 328–344.

Peckham, S. D. (1995), Self-similarity in the geometry and dynamics of large river basins, Ph.D. dissertation, Univ. of Colo., Boulder, Colo.

Pieri, D. C. (1976), Martian channels: Distribution of small channels on the Martian surface, *Icarus*, *27*, 25–50.

Pieri, D. C. (1980), Martian valleys: Morphology, distribution, age, and origin, *Science*, *210*, 895–897.

Pollack, J. B. (1979), Climatic change on the terrestrial planets, *Icarus*, *37*(3), 479–553.

Pollack, J. B., J. F. Kastin, S. M. Richardson, and K. Poliakoff (1987), The case for a wet, warm climate on early Mars, *Icarus*, *71*(2), 203–224.

Rosiek, M. R., R. Kirk, and A. Howington-Kraus (1999), Lunar topographic maps derived from Clementine imagery, *Proc. Lunar Planet. Sci. Conf. 30th*, Abstract 1853.

Schumm, S. A., K. F. Boyd, C. G. Wolff, and W. J. Spitz (1995), A groundwater sapping landscape in the Florida Panhandle, *Geomorphology*, *12*(4), 281–297.

Segura, T. L., O. B. Toon, A. Colaprete, and K. Zahnle (2002), Environmental effects of large impacts on Mars, *Science*, *298*(5600), 1977–1980.

Sharp, R. P., and M. C. Malin (1975), Channels on Mars, *Geol. Soc. Am. Bull.*, *86*(5), 593–609.

Singh, V. P. (1992), *Elementary Hydrology*, 973 pp., Prentice-Hall, Englewood Cliffs, N. J.

Stepinski, T. F., and M. L. Collier (2004), Extraction of Martian valley networks from digital topography, *J. Geophys. Res.*, *109*, E11005, doi:10.1029/2004JE002269.

Stepinski, T. F., and S. Coradetti (2004), Comparing morphologies of drainage basins on Mars and Earth using integral-geometry and neural maps, *Geophys. Res. Lett.*, *31*, L15604, doi:10.1029/2004GL020359.

Stepinski, T. F., and A. P. Stepinski (2005), Morphology of drainage basins as an indicator of climate on early Mars, *J. Geophys. Res.*, *110*, E12S12, doi:10.1029/2005JE002448.

Tarbonton, D. G., L. B. Rafael, and I. Rodrigues-Iturbe (1991), On the extraction of channel networks from digital elevation data, *Hydrol. Processes*, *5*, 81–100.

Williams, R. M. E., and R. J. Phillips (2001), Morphometric measurements of Martian valley networks from Mars Orbiter Laser Altimeter (MOLA) data, *J. Geophys. Res.*, *106*, 23,737–23,752.

————————————

A. D. Howard, Department of Environmental Sciences, University of Virginia, Charlottesville, VA 22903, USA. (ah6p@virginia.edu)

W. Luo, Department of Geography, Northern Illinois University, DeKalb, IL 60115, USA. (wluo@niu.edu)